PCCP

RSC Publishing

PAPER

View Article Online
View Journal | View Issue

Molecular rearrangement reactions in the gas phase triggered by electron attachment†

Cite this: *Phys. Chem. Chem. Phys.*, 2013, **15**, 4754

Benedikt Ómarsson,[a] Elías H. Bjarnason,[a] Sean A. Haughey,[b] Thomas A. Field,*[b] Alexander Abramov,[a] Peter Klüpfel,[a] Hannes Jónsson[a] and Oddur Ingólfsson*[a]

Received 2nd December 2012,
Accepted 6th February 2013

DOI: 10.1039/c3cp44320e

www.rsc.org/pccp

Bond formation and rearrangement reactions in gas phase electron attachment were studied through dissociative electron attachment (DEA) to pentafluorotoluene (PFT), pentafluoroaniline (PFA) and pentafluorophenol (PFP) in the energy range 0–14 eV. In the case of PFA and PFP, the dominant processes involve formation of $[M - HF]^-$ through the loss of neutral HF. This fragmentation channel is most efficient at low incident electron energy and for PFP it is accompanied by a substantial conformational change of the anionic fragment. At higher energy, HF loss is also observed as well as a number of other fragmentation processes. Thermochemical threshold energies have been computed for all the observed fragments and classical trajectories of the electron attachment process were calculated to elucidate the fragmentation mechanisms. For the dominant reaction channel leading to the loss of HF from PFP, the minimum energy path was calculated using the nudged elastic band method.

1. Introduction

Complex chemical reactions in dissociative electron attachment (DEA) studies have until recently received relatively little attention and perhaps have been considered to lie outside the mainstream of the DEA research field. Recent reports[1–10] of electron attachment reactions which involve multiple bond ruptures and new bond formations, at very low electron energies have, however, further accentuated the intrinsic selectivity and dynamic nature of the DEA process. Excellent examples of this type of reactions are the formation of CN^- at around 1.2 eV incident electron energy in DEA to the aliphatic amino acids glycine[1] and valine,[2] and a variety of amides.[3] The formation of CN^- from the amino acids requires at least *five* bond ruptures, which amounts to about 18–19 eV (ref. 2) in bond energy. The energy released in the formation of a CN triple bond from a CN single bond is about 4–5 eV and the electron affinity of the pseudo halogen CN is 3.86 eV.[11] Thus, for this channel to be thermochemically accessible at 1.2 eV incident electron energy, more than 8 eV has to be released by the formation of new bonds. In this context, Papp *et al.*[2] pointed out that the most reasonable path to access these dissociative channels is by the formation of two molecules of hydrogen in the case of glycine and the formation of a hydrogen molecule and a C–H bond to form propane in the case of valine. This is achieved through bond formation between the leaving substituents at the α-C and combination of the two hydrogen atoms from the amine group. A similar reaction is observed in electron attachment to hexafluoroacetoneazine ($(CF_3)_2C{=}N{-}N{=}C(CF_3)_2$),[4] where a variety of DEA fragments are formed through resonances below 1 eV and between 2 and 6 eV. However, in the range between 1 and 2 eV with a maximum at 1.5 eV, CN^- is exclusively formed. This CN^- formation process requires the rupture of three bonds but is still extremely selective with regards to the incident electron energy and only occurs through one, rather narrow low-energy resonance. The only reasonable explanation for this highly efficient channel is the formation of hexafluoroethane ($F_3C{-}CF_3$) through bond formation between the respective terminal CF_3 groups. Furthermore, in DEA to the nucleobase thymine[5] the loss of two hydrogen atoms is the dominant channel close to 0 eV incident electron energy. At such low electron energy this can only be rationalized by the formation of H_2. Another biologically relevant molecule that exhibits this behaviour is the radiosensitized nucleobase 5-chlorouracil[6] (5ClU) where, upon DEA at close to 0 eV incident electron energy, the fragment $[5ClU - HCl]^-$ is observed as a principal fragment. This channel is made thermochemically accessible through the bond energy of 4.5 eV (ref. 12) released in the formation of the halohydride HCl.

[a] *Science Institute, University of Iceland, Dunhagi 3, 107 Reykjavík, Iceland. E-mail: odduring@hi.is; Fax: +354 552 8911; Tel: +354 525 4800*
[b] *Queen's University Belfast, Department of Physics and Astronomy, University Road, Belfast BT7 1NN, N. Ireland, UK. E-mail: t.field@qub.ac.uk; Fax: +44 (0)2890 97 3110; Tel: +44 (0)2890 97 5349*

† Electronic supplementary information (ESI) available. See DOI: 10.1039/c3cp44320e

Evidence for the formation of halohydrides is, however, not limited to the loss of HCl; recent studies[7–9] have shown that the loss of one hydrogen and one fluorine atom leading to the formation of $[M - HF]^-$ can proceed with high efficiency close to 0 eV electron energy in a range of different molecules. These include trifluoroacetic acid,[7] pentafluorophenylacetonitrile,[8] pentafluorophenol and pentafluoroaniline.[9] In all cases the appearance of these fragments at such low energy can only be rationalised by assuming that the channel proceeds through the formation and loss of neutral HF molecules (BDE $\approx$ 5.9 eV (ref. 12)). Hence, these low-energy DEA processes are fuelled by the highly exothermic HF formation.

Generally gas phase DEA studies rely on mass spectrometric detection of the negatively charged fragments formed and no information can be obtained directly about the composition and nature of the complementary neutral fragments formed. What is known in DEA experiments is usually (i) the chemical formula of the target compound, (ii) the mass of the negative ion fragment from which the empirical chemical formula of the negative ion fragment may often be unambiguously deduced, and (iii) the energy dependence of the cross section (ion yield) for the negative ion formation. In direct dissociation, where only one bond is broken the incident electron energy and the electron affinity of the neutral radical, corresponding to the negative ion fragment, must be sufficient to break the bond. It is rarely the case, however, that single bonds can be broken at low incident electron energies, where the attachment cross sections can be very high (10^{-18} to 10^{-16} m^2 at electron energy close to 0 eV (ref. 13). Exceptions are compounds with high electron affinity leaving groups such as Cl, Br, I or CN (see for example the review articles ref. 14 and 15 and references therein). For more complex rearrangement reactions, the energy gained by new bond formation must be taken into account and generally the threshold energy (E_{th}) (*i.e.*, the reaction enthalpy ΔH_{rxn}) for a given DEA process can be approximated by the sum of the bond dissociation energy (BDE) of all bonds broken less the sum of the BDEs of all bonds formed and the electron affinity of the charge-retaining fragment, EA(X). As a result:

$$E_{th}(X^-) \approx \Delta H_{rxn} = \sum_i^N \mathrm{BDE}_i(\mathrm{educt}) - \sum_j^M \mathrm{BDE}_j(\mathrm{product}) - \mathrm{EA(X)} \quad (1)$$

This relationship is useful in the interpretation of DEA data, and often, proposed mechanisms behind the more complex DEA processes can be rationalized through calculations of their thresholds.

In the current paper we have studied electron attachment to the perfluorinated benzene derivatives pentafluorotoluene (PFT); $C_6F_5CH_3$, pentafluoroaniline (PFA); $C_6F_5NH_2$ and pentafluorophenol (PFP); C_6F_5OH in the energy range from 0–14 eV. These compounds show rich fragmentation patterns throughout the energy range and in PFA and PFP low-energy fragmentation channels are observed which can only be rationalized by HF formation, and in the case of PFP, are associated with considerable rearrangement of the aromatic ring. Recently we addressed the role of hydrogen bonds[9] in HF formation from these compounds and we found that the formation of a stabilized, hydrogen bonded intermediate (X···H···F) along the reaction path enables the HF formation from PFA and PFP. Due to the lower polarization of the X–H bond in PFT, on the other hand, no such stabilization is attained and HF loss is not observed.

In the following sections, we discuss the individual fragmentation channels observed in DEA to PFT, PFA and PFP in the energy range from 0–14 eV in the context of the underlying resonances and their lifetimes. By considering the rearrangement of the fragments formed at low incident electron energies, we evaluate the thermochemical thresholds using quantum chemical calculations to aid in the fragment assignment. Furthermore, in recent studies[16–18] we have also used molecular dynamics simulations as a predictive tool to study unimolecular decay processes in fairly large deprotonated biologically relevant molecules. Motivated by the success in the application of these simulations as a predictive tool we apply them here to further elucidate the mechanism behind the more complex fragmentations observed in PFT, PFA and PFP. Finally, we use the nudged elastic band (NEB) method[19,20] to compute the minimum energy path for the dominant reaction channel observed in PFP, which leads to formation of HF and rearrangement of the anionic fragment.

Hence, to understand the reaction pathway from the initial neutral molecule to the fragment ions and the energy dependence of the negative ion formation we; (i) try to narrow down the possible reaction pathways by calculating their thresholds, (ii) use molecular dynamics simulations to predict possible reaction pathways and (iii) compute the minimum energy path from the ground state anion, PFP^-, to a well defined final state, observed in the experiments.

2. Methods

2.1. Electron attachment measurements

The electron attachment experiments were carried out using the Electron Radical Interaction Chamber (ERIC) at Queen's University, Belfast. The instrument has been described in detail elsewhere[21] and we will therefore only give a brief description here. ERIC is a crossed electron beam/time-of-flight mass spectrometer apparatus, in which the electron beam is generated by a pulsed trochoidal electron monochromator (TEM)[22] with a pulse length of approximately 1 μs and a repetition rate of about 10 kHz. The electron energy scale is calibrated with respect to the formation of SF_6^- from SF_6 and the energy resolution, estimated from the FWHM of the SF_6^- signal observed, was found to be ~140 meV. The electron beam interacts with the sample gas in a differentially pumped interaction region. In the current experiment the liquid sample PFT was evaporated through a external gas inlet system into the chamber at room temperature. The solid samples PFA and PFP, on the other hand, were sublimed directly into the reaction chamber through a separate (more direct) inlet system. This has the

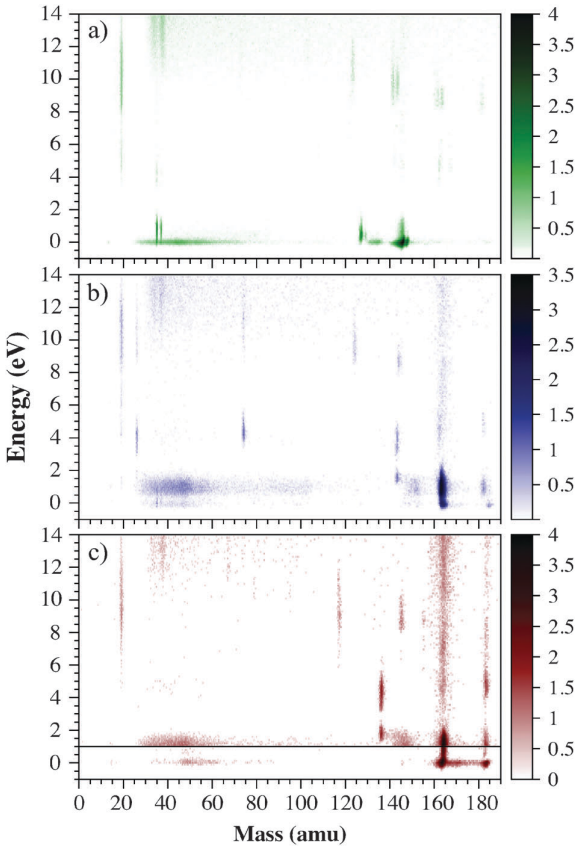

Fig. 1 Two dimensional electron attachment spectra of (a) PFT (182 amu), (b) PFA (183 amu) and (c) PFP (184 amu). The incident electron energy is shown on the vertical axis, ranging from 0–14 eV and the *m*/*z* ratio is displayed on the horizontal axis. The ion intensity is displayed with a gray scale map (colour online) on $\log_{10}$ scale. The horizontal line in the PFP spectrum represents a boundary between different spectra. The high ion intensity close to 0 eV in PFP tends to saturate the multichannel plate detector of the mass spectrometer. The spectra are therefore recorded from 0–14 eV at low pressure and then from 1–14 eV at higher pressure.

consequence that signals from the calibration gas SF_6 as well as trace amounts of other impurities with high DEA cross sections are stronger in the PFT spectra, where the DEA cross sections are low. Furthermore in all M^- ion yield curves some contribution is evident above 0 eV and a broad band primarily located between *m*/*z* 30 and 60 is observed close to 0 eV in all three spectra (see Fig. 1). The former may be attributed to contributions from the $[M - H]^-$ formation, which cannot be totally separated from M^- with the current mass resolution ($\sim$150 $M/\Delta M$ FWHM). The latter is an artifact due to collisions of a small fraction of ions with a grid in the mass spectrometer. In every acquisition cycle, negative ions are generated in the ion source during the 1 μs *on-time* of the TEM. When all electrons have left the source ($\sim$1 μs), ions are extracted by a pulsed electric field of $\sim$200 V cm^{-1} into a region where they are further accelerated (400 V cm^{-1}) into the field free region of the time of flight mass spectrometer (ToF-MS). Finally, the ions are detected with a multichannel plate detector. Pentafluorophenol and pentafluorotoluene were purchased from Sigma Aldrich (St. Louis, MO, USA). Pentafluoroaniline was purchased from Fluorochem (Hadfield, Derbyshire, England). All compounds had a stated purity of 99% and were used as delivered.

2.2. Theoretical calculations

To study possible rearrangement of the fragments formed upon dissociative electron attachment, we used quantum chemical calculations to assess the energy changes in the observed processes. The geometry of the molecules and all neutral and ionic fragments was optimized using density functional theory calculations based on the B3LYP[23,24] hybrid functional approximation and the 6-31G** basis set.[25,26] Vibrational normal mode calculations were then conducted to ensure that an energy minimum had been reached. After that, the energy was calculated using the previously found geometry and the aug-pc-n (n = 0, 1, 2) polarization consistent basis sets[27] along with both B3LYP and B2PLYP[28] functional approximations. The nuclei were assigned velocities to add kinetic energy corresponding to the zero-point energy consistent with the calculated frequencies and thermal vibrational energy at room temperature. Finally, the threshold energy for various channels was calculated by subtracting the total energy of all fragments from the total energy of the respective parent molecule. For each molecule, we tried various final geometries of the fragments formed. Some of these were based on observed fragmentation channels from our classical dynamics simulations (see below), some were based on chemical intuition and some were calculated to allow comparison with energetically unfavourable channels. All the thermochemical calculations were conducted using NWChem 6.0.[29]

To study the mechanism for the formation of the various fragments, Car–Parrinello type molecular dynamics (CPMD) simulations,[30] using the CP2K code,[31] were carried out on the PBE[32] potential energy surface. A plane wave basis set (energy cut-off at 250 Ry) was used with augmented Gaussians from the 6-31G** basis set, *i.e.*, the GAPW method. The influence of core electrons was described by Goedecker–Teter–Hutter (GTH) pseudopotentials[33] as implemented in the CP2K software and the simulations were carried out in a cubic box with 30 Å sides.

In the DEA experiments, the isolated room temperature ground state neutral molecules undergo molecular vibrations as the electron is attached and a transition from the electronic ground state of the neutral molecule to a respective electronic state of the anion is considered to be an instantaneous process. Direct dissociation of a single chemical bond after the attachment of an electron can be achieved within a few vibrational periods whereas an activated process, such as formation of HF and subsequent rearrangement processes can take up to a few microseconds. To speed up the CPMD simulations, kinetic energy of a few electron volts was added by scaling the atomic velocities of the anionic system in the time step where the charge was added (see below). This, however, can also open up new dissociation channels, not accessible at the incident electron energy relevant in the current experiments. The results of such

calculations are, therefore, only meant to give suggestions for the observed fragmentation channels and to identify the corresponding fragments.[16] In the CPMD simulations, the neutral molecules were first optimized to the minimum energy geometry and then simulated as a part of a microcanonical ensemble (NVE) for 1.00 ps in 0.5 fs steps. The temporal variation in energy due to the vibrational motion was Fourier transformed in order to estimate the duration of the longest vibrational period, which was found to be close to 80 fs in most cases. From each of these simulations, we selected 5 different structures for each molecule distributed evenly over this longest vibrational period, *i.e.* structures at t = 0.50, 0.52, 0.54, 0.56 and 0.58 ps were selected. A negative charge was added to the systems as well as kinetic energy corresponding to ~12 eV which was added by scaling the atom velocities. A constant energy (NVE) classical trajectory of the hot, vibrationally excited anion was simulated for a time interval of 2 ps. Several bond ruptures and formation of new neutral or charged molecular species were observed, as described below. When a fragment had travelled far enough to hit the simulation cell boundaries it was removed from the system and the trajectory calculation continued. Finally, the charge of all fragments was determined in each step of the simulation by Mulliken population analysis as implemented in the CP2K code.

In order to elucidate the rearrangement mechanism, we calculated the minimum energy path for the formation of C_5F_4–CO^- from $C_6F_5OH^-$, *i.e.* $[M - HF]^-$, using the nudged elastic band (NEB) method.[19,20] This reaction channel is observed in our classical dynamics simulations and the formation of $[M - HF]^-$ from PFP is the dominant reaction observed in the experiments. These calculations were performed using Chemshell[34] with the NWChem program[29] interfaced as QM code and the DL-FIND[35] program as a geometry optimizer. Due to multiple maxima found on the minimum energy path connecting the initial to the final state, the NEB path was split into three parts, each optimized separately at the B3LYP/6-311+G** level of theory. For each part, a total of 8 images were optimized in addition to the 9th, climbing image[36] which assumes the saddle point geometry.

3. Results and discussions

3.1. DEA to PFT, PFA and PFP

Fig. 1 shows two-dimensional electron attachment spectra of (a) PFT, (b) PFA and (c) PFP. In the case of PFT the DEA cross sections are small and the dominant low-energy contributions are due to background signals of SF_5^- and SF_6^- from the SF_6 calibration gas and Cl^- from trace amounts of impurities (and/or trace background gases). PFA and PFP on the other hand show a rich fragmentation pattern upon DEA. The primary resonances for both these compounds are centred at around 0 eV and around 1 eV.

In all compounds the molecular anion; M^-, is observed close to 0 eV, though the intensities for both PFT and PFA are very low. Hydrogen loss is also observed from PFA and PFP, through the low-energy resonance close to 1 eV, but the dominant contribution from these compounds at low incident electron energies is the loss of one hydrogen and one fluorine atom leading to the mass to charge ratios 163 and 164, respectively. We previously assigned this channel to the formation of $[M - HF]^-$ through neutral HF loss[9] as will be discussed below. The metastable nature of this process is evident for PFP through the line of intensity at 0 eV in the PFP spectrum between m/z 184 and 164, which is due to dissociation of the parent anion; M^-, during acceleration in the mass spectrometer. Further fragmentation is observed from PFA and PFP close to 1.5 eV and 1.8 eV, respectively, and all three compounds show fragmentation through broad but distinct resonances between 3 and 6 eV.

Benzene attaches electrons at 1.15 eV incident electron energy into a degenerate $e_{2u}(\pi^*)$ orbital (LUMO) and at 4.85 eV into a $b_{2g}(\pi^*)$ orbital.[37,38] In substituted benzenes, C_6H_5X; X = OH, NH_2, CH_3,..., the symmetry is lowered from D_{6h} to C_{2v} and the degeneracy of the e_{2u} state is removed. The doubly degenerate $e_{2u}(\pi^*)$ LUMO splits up in an $a_2(\pi^*)$ and a $b_l(\pi^*)$ molecular orbital. In the cases of PFP and PFA the O and N atoms of the –OH and $–NH_2$ groups both have a 2p orbital with b_1 symmetry, which is filled with two electrons. This $b_1(2p)$ orbital interacts with the filled bonding $b_1(\pi)$ and empty antibonding $b_1(\pi^*)$ orbitals on the benzene ring. The net effect is that the $b_1(2p)$ and $b_1(\pi)$ bonding orbitals are stabilized, but the $b_l(\pi^*)$ orbital is destabilized. The stabilization of the occupied $b_1(2p)$ and $b_1(\pi)$ orbitals is the root of the mesomer effect. The $a_2(\pi)$ and $a_2(\pi^*)$ orbitals are of different symmetry and not affected by the $b_1(2p)$ orbital. In toluene, by contrast, the C atom of the $–CH_3$ group has no 2p orbital with a 'lone pair' of electrons that can interact with the $b_1(\pi)$ orbitals. Thus, the two lowest π^* resonances of toluene, with a_2 and b_1 symmetry, are nearly degenerate at 1.1 eV. In aniline they appear at 1.13 and 1.85 eV, respectively, and in phenol they are observed at 1.01 and 1.73 eV, respectively.[38,39] The lower resonances are due to attachment into the unaffected $a_2(\pi^*)$ orbital at energies very close to the toluene resonances, but the higher resonances are due to attachment into the destabilized $b_1(\pi^*)$ orbital. In the molecules investigated here, the situation is further complicated through the fluorine substitution, as the perfluoroeffect[40,41] lowers the energy of the antibonding π^* orbitals only moderately, but has considerably stronger influence on the σ^* orbitals (see for example ref. 42 and 43). In the case of C_6F_5H for example, which should behave similarly to $C_6F_5CH_3$, the lowest lying σ^* orbital is anticipated to be energetically close to the $b_l(2\pi^*)$ MO.[43]

The fluorination of benzene also increases the lifetime of the negative ion states considerably,[44] which is evident through the observation of the molecular anions in our experiment. The long lifetime of the molecular ions will enable a significant portion of the potential energy surface of the anion to be explored by excited species formed in electron attachment prior to dissociation. We thus find it likely that the low-lying resonance close to 0 eV leading to the formation of $[M - HF]^-$ is most appropriately described as a vibrational Feshbach resonance, and that this resonance is associated with an initial

occupation of the $a_1(1\pi^*)$ LUMO. The second contribution in the $[M - HF]^-$ yield from PFA and PFP, on the other hand, is most likely associated with a temporary occupation of the $b_1(2\pi^*)$ or the lowest lying σ^* orbital. In the former case, strong coupling between the $b_1(2\pi^*)$ state and a σ^* orbital(s) may provide the reaction coordinate for dissociation of this negative ion state.

Furthermore, in the electron transmission spectra of toluene, aniline and phenol[38,39] a shape resonance associated with temporary occupation of the $b_1(3\pi^*)$ orbital is observed at 4.88, 5.07 and 4.92 eV, respectively, which correlates well with the observed DEA yields at 5.3 eV in aniline[45] and 5.1 eV in phenol.[46] In pentafluorobenzene, this shape resonance is observed at 4.53 eV in the electron transmission spectra[47] and close to 4.5 eV in DEA.[48] In electron impact excitation of pentafluorobenzene the lowest π–π^* transition is found to be at about 3.9 eV,[49] and in toluene, aniline and phenol the lowest π–π^* transition peaks close to 4.76, 4.41 and 4.59 eV, respectively.[50] In the current study the main contributions in this energy range are from two resonances peaking close to 3.5 eV and 4.5 eV in the ion yields from PFA and PFP. By analogy with the transmission spectra we attribute the higher lying resonance close to 4.5 eV to a shape resonance associated with a temporary occupation of the $b_1(3\pi^*)$ orbital. The lower lying contribution we attribute to a core excited (two-particle–one-hole) resonance associated with the lowest π–π^* transition. Finally, we observe contributions through resonances from 8–12 eV which we assign as two or more core excited resonances.

In the DEA spectra from PFA and PFP the predominant fragmentation channel is the loss of HF through one of the low lying resonances (below 2 eV). This is in apparent contrast to early swarm experiments[51] in which the loss of HF was observed as the most intense signal from PFA, with low intensity from PFT and not at all from PFP. In gas phase negative ion formation through electron attachment, however, the first step can be understood as the formation of a temporary negative ion (TNI) through a transition from the electronic ground state of the neutral molecule to a particular electronic state of the TNI. This transition results in a vibrationally excited TNI (symbolized here by #) if the equilibrium geometry of the neutral precursor differs sufficiently from the equilibrium geometry of the anionic state formed. Under single collision conditions the TNI will have a finite lifetime because loss of an electron to reform the neutral molecule (autodetachment) is an exothermic process and inherently competes with the relaxation of the TNI through dissociation. Hence, within the timeframe of our experiment this TNI can relax either by reemission of the electron:

$$M + e^-(\varepsilon_1) \rightarrow M^{\#-} \rightarrow M^{(\#)} + e^-(\varepsilon_2 \leq \varepsilon_1), \qquad (2)$$

or by dissociation (DEA):

$$M + e^-(\varepsilon_1) \rightarrow M^{\#-} \rightarrow R^{(\#)} + X^-. \qquad (3)$$

In swarm experiments, on the other hand, the pressure of the carrier gas is high and the time between collisions can be of the same order as the life time of relatively short lived negative ion states *e.g.*, 10^{-12} s. Hence, the TNI can lose energy through collisions with the carrier gas (He, Ar, N_2, ...) and relax to its vibrational ground state before dissociation or autodetachment takes place. If the vibrational ground state of the anion formed is below that of the neutral, *i.e.*, if the EA of the neutral precursor is positive, this can lead to relaxation of the TNI to form the thermochemically stable anion before reemission of the electron or dissociation occurs, *e.g.*;

$$M^{\#-} + n\mathrm{He}(\varepsilon_1) \rightarrow M^- + n\mathrm{He}(\varepsilon_2 \geq \varepsilon_1). \qquad (4)$$

This effect becomes clear when we compare the relative cross sections for the loss of HF from PFA and PFP and the observation of the molecular anion M^- in our experiments with the observations in the swarm experiment. In our crossed beam study the formation of $[M - HF]^-$ at low energies dominates from both these compounds, but the intensity of the molecular ion is much higher for PFP (M^- : $[M - HF]^- \approx 1:10$) than for PFA. Furthermore, the metastable nature of the TNI from PFP is also evident through the dissociation of the TNI during the extraction time into the ToF MS (see above). The more prompt decay of the molecular anion from PFA, on the other hand, is evident from the dominating contribution from $[M - HF]^-$ compared to M^- (M^- : $[M - HF]^- \approx 1:250$) and the absence of any sign of dissociation during the extraction into the ToF MS. Correspondingly, the $[M - HF]^-$ fragment from PFA dominates in the swarm experiments while the molecular anion is still observed with appreciable intensity from PFP.

Fig. 2–4 show the energy dependence of the ion yield from DEA to PFT, PFA and PFP in the energy range from 0–14 eV and Table 1 gives the threshold values for the major fragmentation channels calculated for several possible dissociation pathways along with the experimental peak values for the corresponding masses. The threshold values are calculated as described in Section 2.2 and the total energy of each of the molecular species used in the calculations is given in the ESI.† In Fig. 4 (PFP) the displayed spectrum for M^-, $[M - H]^-$ and $[M - HF]^-$ were recorded from 0–14 eV at low pressure to avoid saturation of the detector. Other ion yields, including the inset in the $[M - H]^-$ spectrum, are recorded from 1–14 eV at higher pressure (see Fig. 1).

The most pronounced fragmentation channel from PFA and PFP through the low-energy resonances, is the loss of HF, peaking close to 0 and 1.1 eV in PFA and close to 0 and 0.9 eV in PFP. In the case of PFP the first channel dominates, but in the case of PFA the second dominates. A weak low-energy contribution to the $[M - HF]^-$ signal is also observed from PFT, however, as this is well below the thermochemical threshold we attribute the signal to baseline noise (see Fig. 1). This 0 eV signal is also observed in the F^- ion yield and in the M^- ion yield. However as stated above we find it likely that the 0 eV low intensity M^- signal is actually due to observation of a fraction of the TNI surviving the extraction time in our experiment.

According to our calculations of the thermochemical threshold energies (see Table 1) the loss of a hydrogen and a fluorine

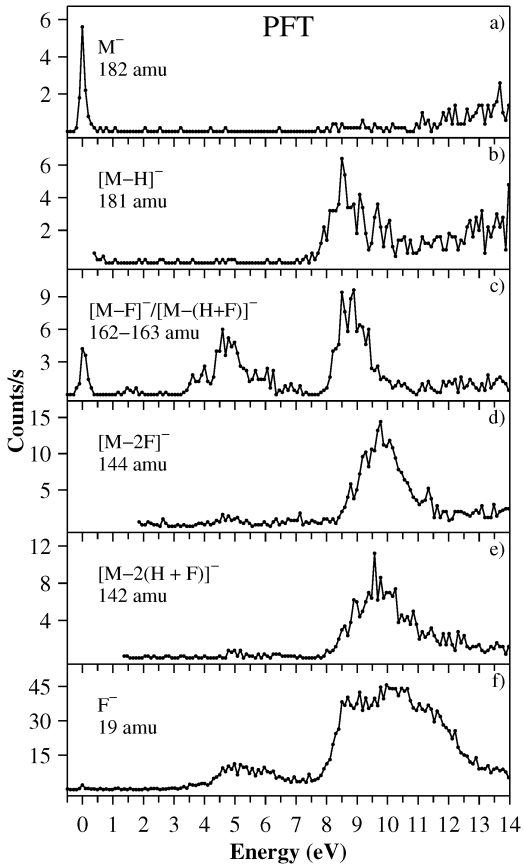

Fig. 2 Ion yield curves from electron attachment to PFT (182 amu) from 0–14 eV incident electron energy. No intense low-energy resonances are observed. The contribution to the M^- signal at 8–14 eV is due to an overlap with the $[M - H]^-$ signal, which cannot be avoided with the current mass resolution. For the same reason the 0 eV M^- signal is also present in the $[M - H]^-$ spectra. For clarity this is not displayed. Furthermore the spectra in panels (d) and (e) are not displayed below 1.5 eV due to overlap with the SF_6^- (146 amu) signal from the calibration gas (see Fig. 1 and discussion in Section 2.1.).

atom below about 6 eV is only possible through the formation of a neutral hydrogen fluoride molecule, *i.e.*, the formation of $[M - HF]^-$.

From PFP this reaction is exothermic by 0.36 eV and 0.19 eV calculated with B3LYP and B2PLYP, respectively, if we assume the formation of HF to be accompanied by rearrangement to a five-membered ring with an exocyclic CO group; C_5F_4–CO^-. For PFA on the other hand we found the most stable final product to be the one where the six-membered ring is retained after the loss of HF. The threshold energy for this reaction is found to be 0.52 and 0.82 eV calculated with B3LYP and B2PLYP, compared to 0.76 eV and 0.96 eV, respectively, if we assume rearrangement to form a five-membered ring with an exocyclic CNH group; C_5F_4–CNH^-. In accordance with our calculations, we assign the formation of $[M - HF]^-$ from PFP close to 0 eV to rearrangement leading to a five-membered ring with a terminal CO group. The $[M - HF]^-$ contribution from PFP close to 0.9 eV, on the other hand, can also result from a final geometry which retains the six-membered ring. From PFA the contribution close to 1.1 eV agrees well with the calculated threshold. The less intense 0 eV contribution however, must be assigned to hot band transitions. These most likely involve the soft vibrational modes of the neutral molecule associated with HF formation as discussed previously.[9]

From threshold calculations for PFP it is clear that the only accessible dissociation channel around 0 eV involves the formation of HF and rearrangement to a five-membered ring. The formation probability of $[M - HF]^-$ from PFP at this energy is thus only controlled by the rate of the reaction compared to the autodetachment rate. The typical extraction time for anions into the ToF MS is several microseconds. The comparatively high intensity of the parent molecular anion thus indicates that the lifetime with respect to autodetachment is fairly long. Hence, the coupling of the electronic state describing this resonance with the vibrational degrees of freedom in the molecule is efficient. Furthermore, in PFP the TNI must couple strongly with the HF formation reaction coordinate, which in turn contributes to stabilization against autodetachment by removing energy from the relevant reaction coordinate. At higher energy, close to 0.9 eV, more energy is available for the dissociation process. The autodetachment rate, however, has also increased and the attachment cross section has diminished. This is evident from the lower intensity of $[M - HF]^-$ from PFP through the higher energy resonance. For PFA the $[M - HF]^-$ formation is energetically not accessible through the 0 eV resonance and there is thus no competition with DEA. Nonetheless the molecular ion is only observed with low intensity. This can be taken as an indication that the coupling between the electronic state involved and the vibrational modes is weaker in PFA than in PFP. Furthermore, as discussed in context to the earlier swarm experiments, the $[M - HF]^-$ formation from PFA through the higher energy resonance (close to 1.1 eV) must be a fairly prompt process, considering the comparatively high intensity of the fragment.

For PFT no hydrogen loss is observed through the low-energy resonances. For PFA and PFP, however, hydrogen loss through the 1.1 eV resonance is observed though far less efficient than the preferred HF loss. The lack of hydrogen loss from PFT through this resonance is readily explainable, as we find the threshold to be 2.02 eV and 2.16 eV calculated with B3LYP and B2PLYP, respectively. In PFA the calculated threshold values are 1.57 eV and 1.48 eV with B3LYP and B2PLYP, respectively, and in PFP these are 0.51 eV and 0.61 eV with B3LYP and B2PLYP, respectively. According to these calculations, the dissociation channel leading to hydrogen loss from PFP is energetically accessible over the whole width of the resonance. This is also the case for hydrogen loss from PFA, as is clear when comparing the $[M - H]^-$ and $[M - HF]^-$ ion yields, through this resonance despite the fact that the calculations yield a slightly higher value for hydrogen loss.

The low intensity of the $[M - H]^-$ fragment compared to the $[M - HF]^-$ fragment can be rationalized by considering the minimum energy geometry for the three compounds PFT, PFA and PFP and the rotational barrier of the respective X–H groups[9] where clear evidence of hydrogen bonding between

Table 1 Threshold calculations for the formation of anionic fragments from different reactions along with the experimentally observed maxima in the ion yield curves for the corresponding masses

	Fragments		ΔH_{rxn} (eV)		Experimental peak positions (eV)	
m/*z*	Anionic	Neutral	B3LYP	B2PLYP	ε_1	ε_2
PFP						
183	$[M - H]^-$	H	0.51	0.61	0.5	4.5
164	$[M - HF]^-/C_5F_4CO^-$	HF	−0.36	−0.19	0	0.9
	$[M - HF]^-/C_6F_4O^-$	HF	0.29	0.59		
	$[M - (H + F)]^-/C_6F_4O^-$	H + F	6.12	6.44		
136	$[M - (CO + HF)]^-/C_5F_4^-$	CO + HF	1.40	1.63	1.5	4.5
PFA						
182	$[M - H]^-$	H	1.57	1.48	1.0	5.0
163	$[M - HF]^-/C_6F_4NH^-$	HF	0.52	0.82	0	1.1
	$[M - HF]^-/C_5F_4CNH^-$	HF	0.76	0.96		
	$[M - (H + F)]^-$	H + F	6.36	6.66		
143	$[M - 2HF]^-/C_5F_3CN^-$	2HF	0.77	0.96	1.5	4.0
	$[M - 2(H + F)]^-/C_6F_3N^-$	2H + 2F	14.76	15.21		
	$[M - 2HF]^-/C_6F_3N^-$	2HF	3.09	3.52		
	$[M - 2(H + F)]^-/C_5F_3CN^-$	2H + 2F	12.44	12.65		
	CN^-	$C_5F_4H + HF$	1.38	1.64	4.0	8–13
	CN^-	$C_5F_4 + H_2$	2.70	3.01		
PFT						
181	$[M - H]^-$	H	2.02	2.16	8.5	
162	$[M - HF]^-$	HF	0.61	0.89	4.5	8.5
162	$[M - (H + F)]^-$	H + F	6.44	6.73		

C–F and H–O in PFP and C–F and H–N in PFA is observed. In the case of PFT, on the other hand, there is no sign of any stabilization. The large dipole moment of the X–H bonds in PFA and PFP thus ensures geometry stabilization through hydrogen bonding, which upon the addition of an electron results in the formation of HF. Hence, the HF formation is enabled through stabilizing X···H···F hydrogen bonding in the neutral precursor, leading to a stabilized intermediate in the HF loss through the DEA process. To further elucidate the progression of this reaction we have calculated the minimum energy path for the HF loss from PFP using the nudged elastic band method and we will discuss these calculations in Section 3.3.

In addition to the HF loss from PFA through the low-energy resonance centred at around 1.1 eV we also observe the loss of two hydrogen atoms and two fluorine atoms with considerable intensities with a threshold close to 1.2 eV. This channel is also observed through two broader, overlapping contributions peaking close to 3.5 and 4.5 eV. We attribute the first contribution to the high-energy tail of the low-energy shape resonance associated with the $b_1(2\pi^*)$ or the lowest σ^* orbital. The latter most likely has contributions both from a shape resonance associated with occupation of the $b_1(3\pi^*)$ orbital and the formation of a core excited resonance associated with a low lying π–π^* transition. Energetically these fragmentation channels are not accessible without the formation of two HF molecules, and for the $[M - 2HF]^-$ formation from PFA we derive thresholds of 0.77 and 0.96 eV with B3LYP and B2PLYP, respectively, if we assume that the reaction takes place by the formation of two HF molecules and a rearrangement of the charge-retaining fragment to form a five-membered ring with an exocyclic CN group. If, however, the six-membered ring stays intact and the only energy gain for this reaction comes through the formation of two HF molecules, we find thresholds of 3.09 eV and 3.52 eV with B3LYP and B2PLYP, respectively. The experimental threshold for this reaction through the low-energy contribution agrees well with the calculated threshold for the reaction path leading to a five-membered ring with an exocyclic CN group. Given the experimental and computational uncertainties, $[M - 2HF]^-$ formed through the higher-energy resonances may result from both these channels, *i.e.*, with a resulting five-membered or six-membered ring structure.

From PFP we observe a similar ion yield curve for the formation of the fragment $[M - (HF + CO)]^-$ as is observed for the formation of $[M - 2HF]^-$ from PFA, *viz.* a comparatively narrow contribution with an onset at about 1.2 eV and broader overlapping contributions close to 3.5 and 4.5 eV. Similar to PFA we assign these contributions to the high-energy tail of the low-energy shape resonance centred at about 0.9 eV and to the higher lying resonances discussed above. If we assume this reaction to be combined with rearrangement of the charge-retaining fragment to form an open shell five-membered ring we calculate the threshold to be 1.40 and 1.63 eV with B3LYP and B2PLYP, respectively. An open chain configuration of the charge-retaining fragment, on the other hand, leads to thresholds of 2.83 and 3.26 eV with B3LYP and B2PLYP, respectively. The low-energy $[M - (HF + CO)]^-$ formation from PFP must thus be associated with the formation of a five-membered ring. This is analogous to the lower energy contribution of $[M - 2HF]^-$ formation from PFA, which also requires five-membered ring formation. The open chain configuration of the charge-retaining fragment may, however, contribute to $[M - (HF + CO)]^-$ formation at higher energy.

In addition to the low-energy contributions (below 2 eV) and the $[M - HF]^-$ formation from PFA at around 3.5 and 4.5 eV,

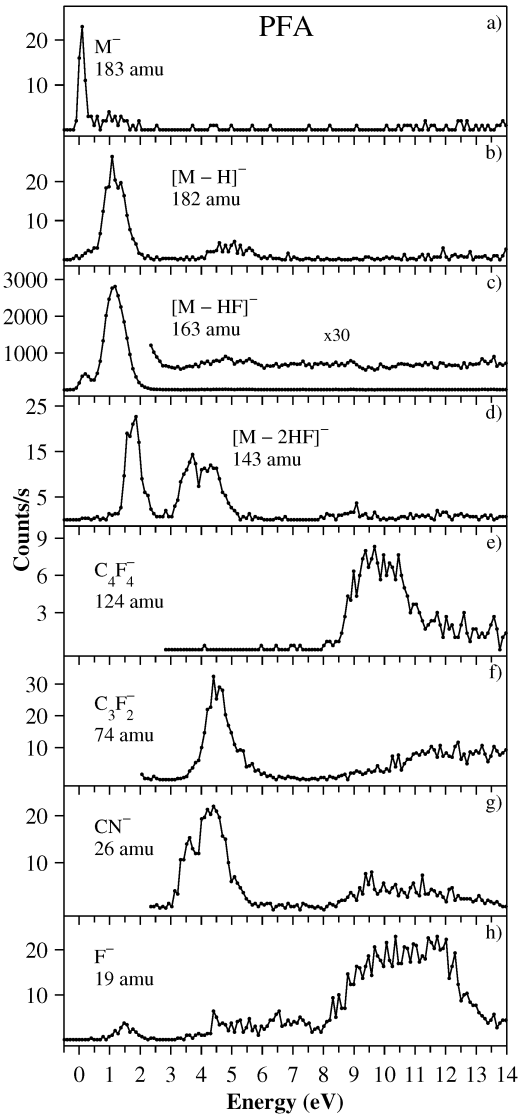

Fig. 3 Ion yield curves from electron attachment to PFA (183 amu) from 0–14 eV incident electron energy. The highest contribution observed is the $[M - HF]^-$ fragment close to 0 eV, formed by the loss of neutral HF. Also observed is the formation of $[M - 2HF]^-$ and CN^-. For clarity, the spectra in panels (e), (f) and (g) are not displayed below 2 eV due to overlap with the broad background signal (see Fig. 1 and discussion in the text).

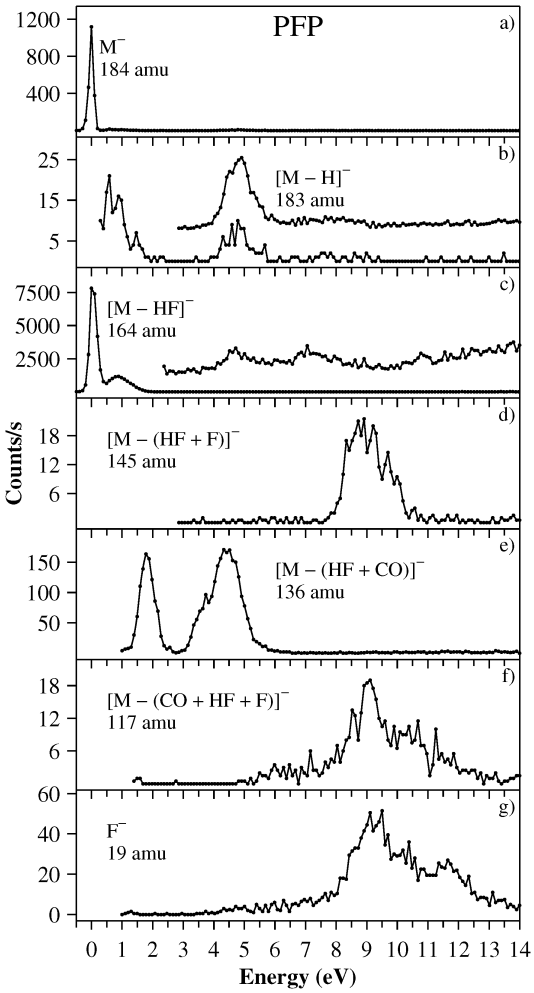

Fig. 4 Ion yield curves from electron attachment to PFP (184 amu). The highest contribution observed is the $[M - HF]^-$ fragment close to 0 eV, formed by the loss of neutral HF. The molecular ion is also formed with considerable intensity near 0 eV. The formation of $[M - (HF + CO)]^-$ is observed through 2 resonances. The spectra in panels (a)–(c) are recorded at low pressure and the spectra in panels (d)–(g) and the inset in panel (b) are recorded at higher pressure. To avoid saturation of the detector at low incident electron energies these are only recorded from 1 eV. Below this energy, however, these fragments are not formed (see Fig. 1 and discussion in the text).

we also observe the formation of $C_3F_2^-$ and CN^- from PFA through the two overlapping resonances close to 3.5 and 4.5 eV. In the case of the CN^- formation our calculations give threshold energies of 1.38 and 1.64 eV with B3LYP and B2PLYP, respectively, if the reaction involves the formation of HF and a transfer of the second hydrogen from the nitrogen to the carbon in the *ortho* position, which was vacated by the fluorine atom of HF. If we assume H_2 formation from the amine group, however, and the formation of perfluorocyclopentadiene, the threshold for this reaction is found to be 2.70 and 3.01 eV with B3LYP and B2PLYP, respectively. The experimental appearance energy for this reaction is close to 3.0 eV, and both of these channels are thus accessible at these energies. It is important to point out here that the observation of experimental appearance energy above the theoretical threshold does not rule out a process, which may not appear at its thermochemical threshold for a number of reasons. By contrast, if the appearance energy is significantly lower than a calculated thermochemical threshold it is strong evidence that a lower energy channel to the same product is available.

Finally, in the case of PFT, the core excited resonances ranging from 8–12 eV lead to the formation of the anionic fragments $[M - F]^-$, $[M - H]^-$ and F^-. These fragments can all be formed through single bond rupture, but also the fragment ions $[M - 2F]^-$, $[M - (H + F)]^-$ and $[M - 2(H + F)]^-$ are observed

in this energy range. With the exception of $[M - 2(H + F)]^-$ all these fragmentation channels are thermochemically accessible at this energy, and there is no indication that they are associated with rearrangement processes or new bond formation. The loss of two hydrogen atoms and two fluorine atoms from PFT, on the other hand, is likely to be associated with at least the formation of one neutral HF. From PFA we also observe F^- and $[M - H]^-$ formation from these resonances and additionally more complicated fragmentation processes leading to the formation of $C_4F_4^-$, $C_3F_2^-$ and CN^-. The three latter fragments all require a carbon excision from the aromatic ring with at least two C–C bond ruptures. From PFP the fragments F^- and $[M - H]^-$ are observed through these high-energy resonances and additionally the fragments $[M - (2F + H)]^-$ and $[M - (F + H + C + O)]^-$. The latter is likely to be formed through rearrangement involving neutral HF and/or CO formation (see above).

3.2. Simulations of the fragmentation of the PFT, PFA and PFP molecular anions in their electronic ground state

To further elucidate the dynamics of the dissociation processes, we have conducted classical dynamics simulations of the fragmentation of the PFT, PFA and PFP molecular anions.

These simulations are a rather rough representation of the experimental conditions and only five initial geometries were chosen for each molecule. Nonetheless, the simulations reproduce remarkably well the main fragmentation channels observed in our experiments and are a valuable tool for suggesting possible mechanisms and help interpret the experimental data. Fig. 5–7 depict the observations from the classical dynamics simulations of the PFT, PFA and PFP molecular anions, respectively. The coordinate files are available in the ESI.† For PFT (Fig. 5), two out of five simulations showed rapid loss of the *para*-fluorine at the beginning of the simulation. Loss of the *meta*-fluorine was observed in another two out of the five simulations, but these occurred after 1–2 ps. In the fifth trajectory, loss of the *ortho*-fluorine and HF formation was observed.

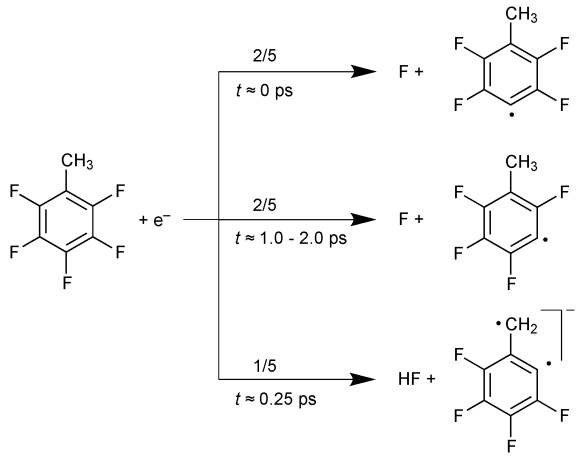

Fig. 5 Results of classical dynamics simulations for the PFT anion. A total of five trajectories were calculated and three different fragmentation channels were observed.

This fragmentation channel proceeds within about 0.25 ps and leaves the remaining fragment as a planar six-membered ring. Apparently, the loss of HF from PFT does not proceed through stabilized hydrogen bonds, but is the result of a fluorine loss and subsequent (coincidental) hydrogen abstraction from the CH_3 group by the free fluorine atom (see ESI†). The most pronounced product ions observed from PFT in the energy range from about 4–6 eV are F^- and $[M - F]^-$, but no fragmentation is observed directly from the anionic ground state of PFT in our experiment. We have however, no means to judge if the final fragmentation processes proceed from the originally formed excited states or after conversion to the respective ground states. In our experiments, all fragmentation channels from PFT, other than the fluorine loss, are observed predominantly above 8 eV. The simulations thus reproduce fairly well the experimentally observed fragmentation pattern of PFT.

Fig. 6 shows the observed fragmentation channels from the classical dynamics simulations of the PFA anion. In good agreement with the experimental observations, three out of the five trajectories for PFA led to the loss of HF through a stabilized hydrogen bonded N···H···F intermediate. These reactions occurred within 0.2–0.5 ps. In two of them, the remaining fragment retains the planar six-membered ring geometry. In the third, a further rearrangement takes place after the HF loss (after about 0.85 ps) and the final geometry of the remaining fragment is a five-membered ring with an exocyclic CNH group. In the other two trajectories, an immediate fluorine loss was observed; in one case from the *ortho*- and in the other case from the *meta*-position. These simulations reproduce the dominant low-energy formation of $[M - HF]^-$ from PFA well. At higher energy, with a threshold close to 1.2 eV the experiments show a fairly intense loss of two HF molecules but this does not occur in the simulations, possibly due to the short simulation time. The present simulations were run for 2 ps as the computational effort required for longer trajectories of, for example, 1 ns or 1 μs is not affordable. Finally, the (instant) cleavage of the C–F bonds observed in our simulations, is reflected in our experiments through resonances in the energy range of about 4–8 eV and above 8 eV.

Fig. 7 shows the fragmentation channels observed in classical dynamics simulations of the PFP anion. In one out of five trajectories OH was lost from the molecule. The resulting fragment is stable but we observe large C–F vibrational amplitudes, indicating that further fragmentation might occur on a longer time scale. This fragmentation process is not observed in our experiments. In four out of the five trajectories, HF loss is observed through a stabilized O···H···F intermediate involving the *ortho*-fluorine. In one out of these four simulations, however, the loss of a fluorine atom from the *meta*-position within the first 0.2 ps precedes the loss of HF. In this case, the final geometry retains the planar six-membered ring. In two of the remaining cases, loss of HF proceeds within the first 0.25 ps and in the last case within 1.0 ps. In these trajectories, the HF loss is followed by rearrangement of the ring within about 1.0–1.3 ps from the start of the simulation. In one of them,

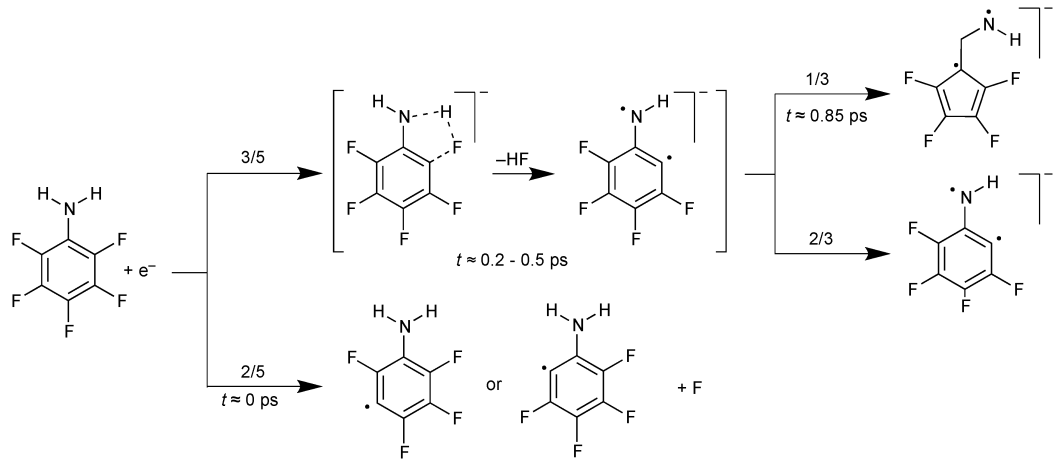

Fig. 6 Results of classical dynamics calculations for the PFA anion. A total of five trajectories were calculated and three different fragmentation channels were observed.

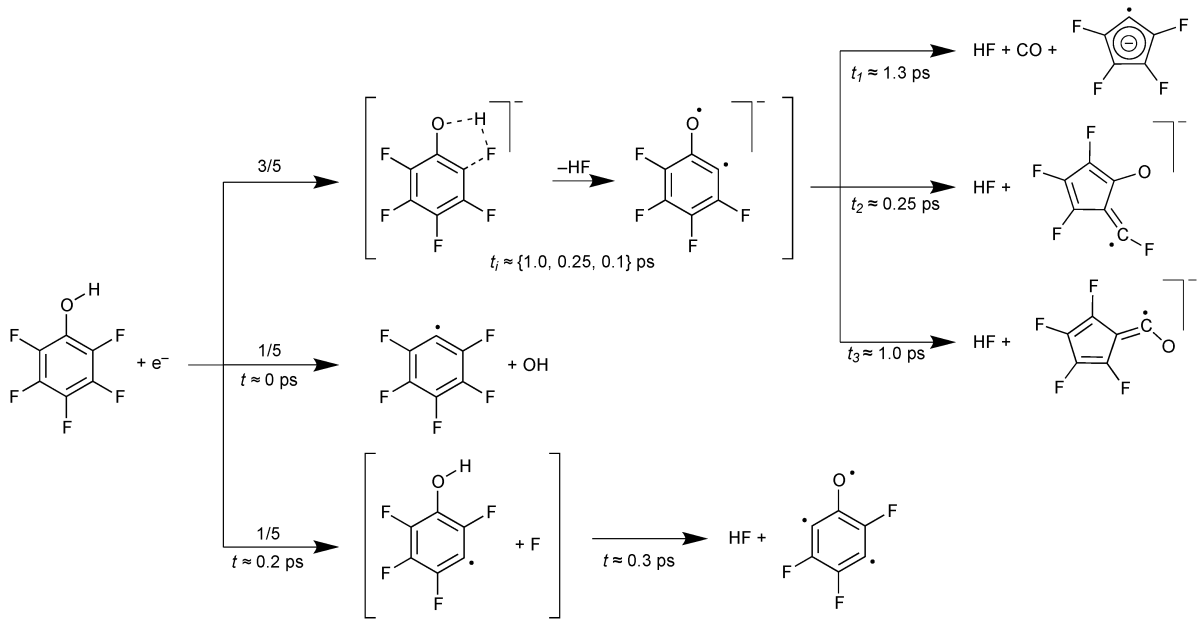

Fig. 7 Results of classical dynamics calculations for the PFP anion. A total of five trajectories were calculated and four different fragmentation channels were observed.

the rearrangement process leads to the additional loss of CO subsequent to the HF loss and the formation of the aromatic tetrafluoro-cyclopentadienyl anion radical. In another, the fragmentation process halts at the tetrafluoro-cyclopentadienyl where the exocyclic CO group is still attached. Finally in the third, the rearrangement leads to a five-membered ring with the oxygen attached to the ring and a fluorine on the exocyclic carbon (see Fig. 7). In the first two cases the closure of the five-membered ring proceeds through bond formation between C2 and C6 of the initial benzene ring. In the third case, the bond formation proceeds through C2 and C4 of the initial benzene ring. These simulations reflect the dominant role of the HF formation in DEA to PFP and agree well with our experimental observations. Furthermore, the simulations also reproduce the complicated rearrangement after loss of one HF and even the additional loss of CO from PFP. This latest channel is observed in our experiments with fairly high intensity through the high-energy side of the second low-energy resonance located close to 0.9 eV. From our thermochemical calculations it is clear that this channel is only accessible through the formation of the cyclopentadiene anion as is observed in our simulations.

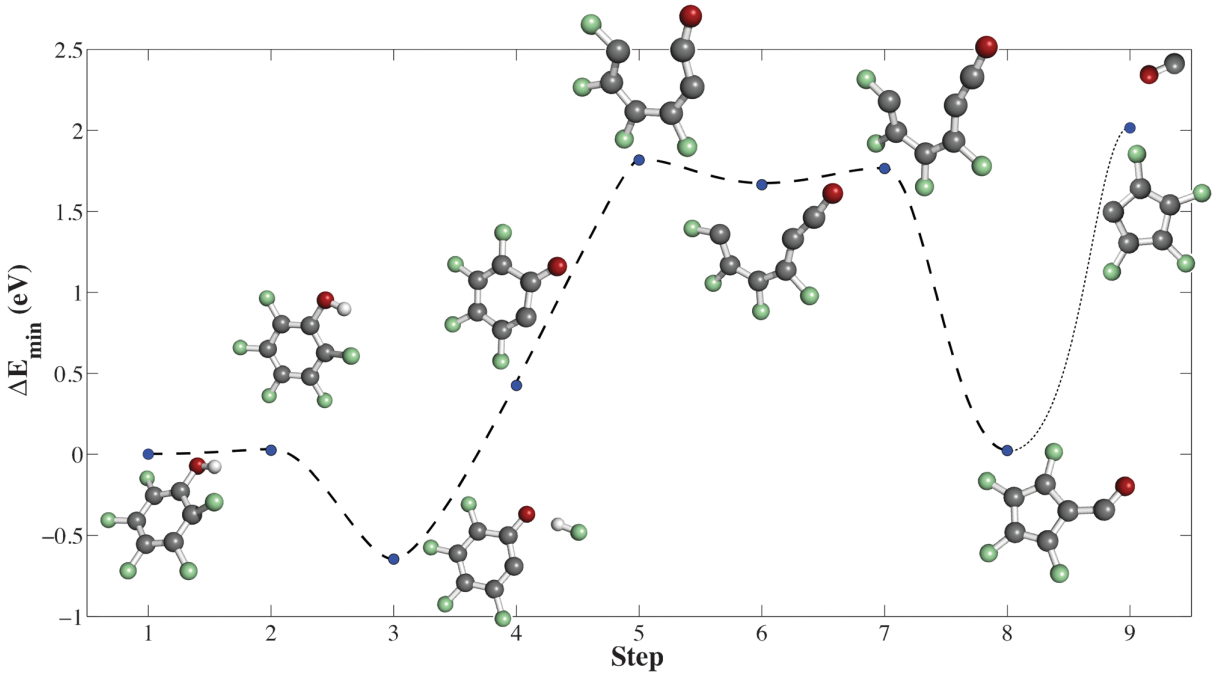

Fig. 8 The minimum energy path for the formation of $C_5F_4CO^-$ (step 8) from the ground state of $C_6F_5OH^-$ (step 1) on the B3LYP/6-311+G** potential energy surface, calculated using the NEB method. The last point in the figure, step 9, corresponds to the additional loss of CO, forming $[M - HF - CO]^-$ (see Section 3.1).

3.3. Nudged elastic band calculations

The dominant contribution in DEA to PFP is the formation of $[M - HF]^-$ through a resonance centred close to 0 eV. We have shown by thermochemical calculations that the final state of this fragment is a pentagonal structure with a terminal CO group. Furthermore, the classical trajectories reported in the previous section yield this product in one out of five simulations.

Fig. 8 shows the calculated minimum energy path, on the B3LYP potential energy surface (PES), for the formation of $C_5F_4CO^-$ (step 8) from the ground state of $C_6F_5OH^-$ (step 1). Each point represents either a calculated minimum or a saddle point on the PES, but the dashed line is only meant to guide the eye and does not necessarily follow the computed path. For completeness we included, as the final step, the energy of the system after additional loss of CO, *i.e.*, formation of the stable cyclopentadienyl radical. This fragment is observed in the experiment, peaking at around 1.8 eV, and also in the classical dynamics simulations. From Fig. 8 it is evident that the hydrogen bonded intermediate depicted in step 3 is favoured over the molecular anion. It should be noted here that if this complex survives the extraction into the field free region of the mass spectrometer it will be detected as the molecular anion. Furthermore, the reaction leading to the formation of this intermediate state proceeds with an energy barrier of less than 0.1 eV. Proceeding from step 3, we assume HF is separated from the system and add the HF energy to the energy of the computed fragments. In step 4 and onwards, the molecule opens up, by dissociation of the C1–C6 bond, forming an unstable open chain structure and finally rearranges to the 5-membered $C_5F_4CO^-$ anion *via* bond formation between C6 and C2.

The classical trajectory calculated for the DEA process, where the same final state was observed, revealed a similar reaction path. However, formation of the 5-membered ring in the classical dynamics simulations (though initiated through a C1–C6 bond rupture) results from C6–C2 bond formation after rotation of the C1–C2 bond. Rotation, however, is hindered along the minimum energy path, and the height of the energy barrier is a good indication of the observed metastable nature of the $[M - HF]^-$ formation in PFP. For the classical trajectory to proceed through the minimum energy path, the calculations should be performed without the addition of kinetic energy. The height of the reaction barrier however results in a low rate and the reaction time is therefore too long for it to be feasible to observe a reaction event in the simulations without the addition of kinetic energy.

4. Conclusions

The attachment of a single low-energy electron ($\varepsilon < 2$ eV) to PFA and PFP primarily leads to reactions involving the formation of HF. Further reactions involving rearrangement of the remaining anionic fragment have also been identified. These are often quite complex such as the loss of HF and CO from PFP, the loss of two HF molecules from PFA and the CN^- formation from PFA. For the compounds presented here, we assign the ability of PFA and PFP to form intermolecular

hydrogen bonds as a prerequisite for the formation of HF upon electron attachment. The polarized nature of the O–H and N–H bonds ensures a strong interaction with a neighbouring fluorine atom. We have successfully utilized classical dynamics simulations to better understand the mechanism behind the formation of HF as well as further rearrangement of the anionic fragment. The classical trajectories, although calculated by adding considerable kinetic energy to the system, reproduce the experimental observations well. Furthermore, the results give valuable insight into the mechanism of complex chemical reactions triggered by a single low-energy electron in gas phase electron attachment experiments.

Acknowledgements

The authors acknowledge financial support from the Icelandic Centre for Research (RANNIS), the University of Iceland Research Fund, the EPSRC and the Royal Society. B.O., E.H.B. and O.I. acknowledge support for a visit to Belfast by the European Network ITS-LEIF. Special thanks goes to Ragnar Björnsson for technical assistance concerning calculations. This work was conducted within the framework of the COST action CM0601 on electron controlled chemical lithography.

Notes and references

1 A. Mauracher, S. Denifl, A. Aleem, N. Wendt, F. Zappa, P. Cicman, M. Probst, T. D. Märk, P. Scheier, H. D. Flosadóttir, O. Ingólfsson and E. Illenberger, *Phys. Chem. Chem. Phys.*, 2007, **9**, 5680–5685.
2 P. Papp, J. Urban, S. Matejčík, M. Stano and O. Ingólfsson, *J. Chem. Phys.*, 2006, **125**, 204301.
3 C. Koenig-Lehmann, J. Kopyra, I. Dbkowska, J. Kočišek and E. Illenberger, *Phys. Chem. Chem. Phys.*, 2008, **10**, 6954.
4 I. Bald, I. Dbkowska, E. Illenberger and O. Ingólfsson, *Phys. Chem. Chem. Phys.*, 2007, **9**, 2983.
5 S. Denifl, S. Ptasinska, M. Probst, J. Hrusak, P. Scheier and T. D. Märk, *J. Phys. Chem. A*, 2004, **108**, 6562–6569.
6 S. Denifl, S. Matejčík, B. Gstir, G. Hanel, M. Probst, P. Scheier and T. D. Märk, *J. Chem. Phys.*, 2003, **118**, 4107.
7 J. Langer, M. Stano, S. Gohlke, V. Foltin, S. Matejčík and E. Illenberger, *Chem. Phys. Lett.*, 2006, **419**, 228–232.
8 I. Dbkowska, H. D. Flosadóttir, M. Orzol, S. Ptasinska, I. Bald, O. Ingólfsson and E. Illenberger, *Phys. Chem. Chem. Phys.*, 2009, **11**, 5323–5330.
9 B. Ómarsson, E. H. Bjarnason, S. Haughey, T. A. Field and O. Ingólfsson, *Chem. Phys.*, 2012, **539–540**, 7.
10 P. Sulzer, F. Rondino, S. Ptasinska, E. Illenberger, T. D. Märka and P. Scheier, *Int. J. Mass Spectrom.*, 2008, **272**, 149–153.
11 S. E. Bradforth, E. H. Kim, D. W. Arnold and D. M. Neumark, *J. Chem. Phys.*, 1993, **98**, 800–810.
12 Y.-R. Luo, *Comprehensive Handbook Of Chemical Bond Energies*, 2007.
13 L. G. Christophorou and J. K. Olthoff, *Appl. Surf. Sci.*, 2002, **192**, 309–326.
14 I. Bald, J. Langer, P. Tegeder and O. Ingólfsson, *Int. J. Mass Spectrom.*, 2008, **277**, 4–25.
15 O. Ingólfsson, F. Weik and E. Illenberger, *Int. Rev. Phys. Chem.*, 1996, **15**, 133–151.
16 H. Flosadóttir, B. Ómarsson, I. Bald and O. Ingólfsson, *Eur. Phys. J. D*, 2012, **66**, 1–20.
17 H. D. Flosadóttir, S. Denifl, F. Zappa, N. Wendt, A. Mauracher, A. Bacher, H. Jónsson, T. D. Märk, P. Scheier and O. Ingólfsson, *Angew. Chem., Int. Ed.*, 2007, **46**, 8057–8059.
18 H. D. Flosadóttir, H. Jónsson, S. T. Sigurdsson and O. Ingólfsson, *Phys. Chem. Chem. Phys.*, 2011, **13**, 15283.
19 H. Jónsson, G. Mills and K. W. Jacobsen, in *Classical and Quantum Dynamics in Condensed Phase Simulations*, ed. G. C. D. F. C. B. J. Berne, World Scientific, Singapore, 1998, p. 385.
20 H. Jónsson, *Proc. Natl. Acad. Sci. U. S. A.*, 2011, **108**, 944–949.
21 T. A. Field, A. E. Slattery, D. J. Adams and D. D. Morrison, *J. Phys. B: At., Mol. Opt. Phys.*, 2005, **38**, 255–264.
22 A. Stamatovic and G. J. Schulz, *Rev. Sci. Instrum.*, 1968, **39**, 1752–1753.
23 A. D. Becke, *J. Chem. Phys.*, 1993, **98**, 5648–5652.
24 C. T. Lee, W. T. Yang and R. G. Parr, *Phys. Rev. B: Condens. Matter Mater. Phys.*, 1988, **37**, 785–789.
25 P. C. Hariharan and J. Pople, *Theor. Chim. Acta*, 1973, **28**, 213.
26 W. J. Hehre, R. Ditchfield and J. A. Pople, *J. Chem. Phys.*, 1972, **56**, 2257–2261.
27 F. Jensen, *J. Chem. Phys.*, 2002, **117**, 9234–9240.
28 S. Grimme, *J. Chem. Phys.*, 2006, **124**, 034108.
29 M. Valiev, E. J. Bylaska, N. Govind, K. Kowalski, T. P. Straatsma, H. J. J. Van Dam, D. Wang, J. Nieplocha, E. Apra, T. L. Windus and W. A. de Jong, *Comput. Phys. Commun.*, 2010, **181**, 1477–1489.
30 R. Car and M. Parrinello, *Phys. Rev. Lett.*, 1985, **55**, 2471.
31 CP2K version 2.1.362 (Development Version), the CP2K developers group: http://www.cp2k.org.
32 J. P. Perdew, K. Burke and M. Ernzerhof, *Phys. Rev. Lett.*, 1997, **78**, 1396.
33 S. Goedecker, M. Teter and J. Hutter, *Phys. Rev. B: Condens. Matter Mater. Phys.*, 1996, **54**, 1703.
34 ChemShell, a Computational Chemistry Shell, see www.chemshell.org.
35 J. Kästner, J. M. Carr, T. W. Keal, W. Thiel, A. Wander and P. Sherwood, *J. Phys. Chem. A*, 2009, **113**, 11856–11865.
36 G. Henkelman, B. P. Uberuaga and H. Jónsson, *J. Chem. Phys.*, 2000, **113**, 9901–9904.
37 L. Sanche and G. J. Schulz, *J. Chem. Phys.*, 1973, **58**, 479–493.
38 K. D. Jordan, J. A. Michejda and P. D. Burrow, *J. Am. Chem. Soc.*, 1976, **98**, 7189–7191.
39 K. D. Jordan, J. A. Michejda and P. D. Burrow, *J. Am. Chem. Soc.*, 1976, **98**, 1295–1296.
40 C. R. Brundle, M. B. Robin, N. A. Kuebler and H. Basch, *J. Am. Chem. Soc.*, 1972, **94**, 1451–1465.
41 C. R. Brundle, M. B. Robin and N. A. Kuebler, *J. Am. Chem. Soc.*, 1972, **94**, 1466–1475.

42 P. Decleva, M. Stener, D. M. P. Holland, A. W. Potts and L. Karlsson, *J. Phys. B: At., Mol. Opt. Phys.*, 2007, **40**, 2939.
43 A. P. Hitchcock, P. Fischer, A. Gedanken and M. B. Robin, *J. Phys. Chem.*, 1987, **91**, 531–540.
44 L. G. Christophorou, The Lifetimes of Metastable Negative Ions, in *Advances in Electronics and Electron Physics*, ed. L. Marton, Academic Press, New York, 1978, vol. 46, pp. 55–129.
45 S. Pikhtovnikov, V. Mavrodiev, I. Furley, R. Gataullin and I. Abdrakhmanov, *High Energy Chem.*, 2006, **40**, 224–229.
46 M. V. Muftakhov, R. V. Khatymov and V. A. Mazunov, *Rapid Commun. Mass Spectrom.*, 2000, **14**, 1468–1473.
47 J. R. Frazier, L. G. Christophorou, J. G. Carter and H. C. Schweinler, *J. Chem. Phys.*, 1978, **69**, 3807–3818.
48 H.-P. Fenzlaff and E. Illenberger, *Int. J. Mass Spectrom. Ion Processes*, 1984, **59**, 185–202.
49 R. P. Frueholz, W. M. Flicker, O. A. Mosher and A. Kuppermann, *J. Chem. Phys.*, 1979, **70**, 3057–3070.
50 T. Ari, H. Güven and N. Ecevit, *J. Electron Spectrosc. Relat. Phenom.*, 1995, **73**, 13–23.
51 I. Gregor and M. Guilhaus, *J. Fluorine Chem.*, 1983, **23**, 549–556.

